Fachtagung "Experimentelle Strömungsmechanik"
5.–7. September 2023, München

Temperature measurement on an SD7003 airfoil using the single-shot lifetime method in a towing tank

Temperaturmessung an einem SD7003-Profil mittels der Single-Shot Lifetime Methode in einem Schleppkanal

Tudor V. Venenciuc[1], Christian Klein[2], Rainer Hain[1], Christian J. Kähler[1]
1: Institut für Strömungsmechanik und Aerodynamik, Universität der Bundeswehr München, Neubiberg 85577, Deutschland
2: Institut für Aerodynamik und Strömungstechnik, Deutsches Zentrum für Luft- und Raumfahrt (DLR), Bunsenstrasse 10, Göttingen, 37073, Deutschland

Keywords: SD7003, Airfoil, TSP, single-shot lifetime, towing tank
Schlagworte: SD7003, Profil, TSP, Single-Shot Lifetime, Schleppkanal

Abstract

Time-resolved surface temperature measurements on the suction side of an SD7003 airfoil at a Reynolds number of 60000 were successfully performed in a towing tank. The experiments were able to confirm the suitability of the single-shot lifetime method for studying the unsteady fluid dynamic phenomenon associated with laminar separation bubbles. To facilitate the visualization of the thermal fluctuations induced by the periodic vortex shedding, a carbon-based electrically conductive paint is sprayed on the suction side of the wing. The footprints of Kelvin-Helmholtz vortices were observed by this method at angles of attack of α=2˚, 4˚, 6˚, and 8˚. The spanwise coherence of the vortices is high enough that their footprints on the model surface are still visible after spanwise averaging the thermal signal. This compensates for the low fluctuation amplitudes and improves the readability of the spectral content.

1. Introduction

Phosphorescent molecules have been used as a substitute for infrared thermography (Liu et al. 2021) in numerous academic studies over the past decades. The use of temperature-sensitive paints (TSP) allow the non-invasive study of temperature distribution on almost any surface. However, disadvantages such as photodegradation, unstable excitation illumination patterns, or low signal-to-noise ratio have limited the use of the measurement method for many years. The development of cameras with more light sensitive sensors, stronger and cheaper light sources but also luminescent dyes with higher emissivity have improved the sensitivity of the measurement method and extended the range of applications in the past years. Time-resolved temperature reads have thus been able to provide insight into the complex fluid mechanical processes that could previously only be studied at low resolutions. Lemarechal et al. 2018 were able to observe in detail the formation and propagation of turbu-

GALA e.V., Karlsruhe, Germany, ISBN 978-3-9816764-9-5

lent spots. For this purpose, a heatable surface was sprayed with TSP and the footprints of vortical structure on the thermal field were analyzed. The approach can also be used on curved surfaces as shown by Miozzi et al. 2016. They were able to detect the footprints of Görtler instabilities on a cylindrical surface. The experimental work was conducted in a facility in which the illumination pattern could remain constant though. As soon as disturbing elements like model vibrations, time-varying light reflections, or impurities in the flow medium occur, the variation of the illumination intensity has to be corrected or eliminated. One possible solution is the use of so-called binary paints, which consist of one molecule that is sensitive to temperature or pressure and another that responds only to differences in excitation patterns. Another solution is the lifetime method. Photoluminescent molecules exhibit both fluorescent and phosphorescent properties. Thermal quenching reduces the emitted light of an excited molecule at elevated temperatures. The lifetime method can be used to measure temperature without the need for a reference state. The method is less sensitive to photodegradation, illumination variation, or dye concentration differences (Liu et al. 2021), but is known for its low signal-to-noise ratio. However, a few years ago, a temperature-sensitive Europium-based molecule was discovered that exhibits excellent lifetime properties. This is used in the present work in a towing tank with the aim of studying on the suction side of an SD7003 airfoil the footprints of coherent flow structures formed at low Reynolds numbers (Re_c), at which laminar separation bubbles occur.

2. The experimental setup and the towing tank

The experiments are performed in the towing tank at the University of the Bundeswehr Munich. The volume measures of 8^{L} x 0.9^{H} x 0.9^{W} m^3. A total of 5 m of the 8 m of the length are equipped with glass windows allowing optical access from the side and below the tank. On the two rails, which are parallel to the length of the tank, the carriage, to which the measuring instruments and the hydrofoil are fixed, is placed. Figure 1 shows several pictures displaying the setup.

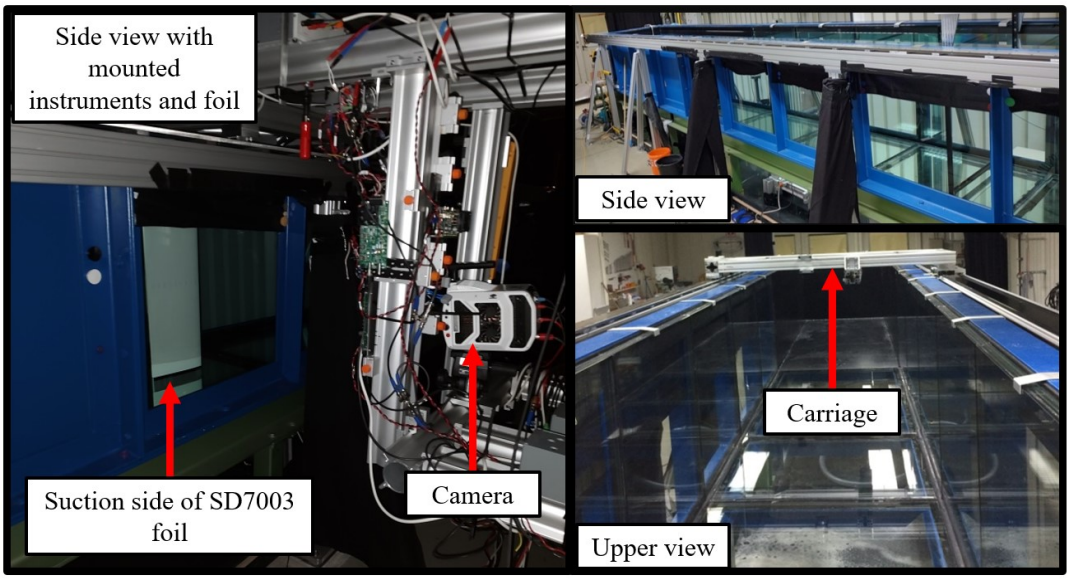

Fig. 1. Images of the towing tank with and without mounted foil, temperature detection system and water

The carriage is connected to a belt, which in turn is driven by a servo motor. The velocity oscillations without the wing installed are shown in figure 2.
The SD7003 airfoil has a chord length c=250 mm and consists partly of aluminum for stability reasons and acrylic glass for the electrical insulation at the measured location. The two ma-

GALA e.V., Karlsruhe, Germany, ISBN 978-3-9816764-9-5

terials are glued together before being milled to form the foil. On the suction side, a 0.1 mm deep groove is milled. In addition, two narrower 0.035 mm deep grooves are milled, onto which copper tapes are placed. A CAD model of the wing, geometric dimensions and heating element components can be seen in figure 3. The tapes are guided around the leading edge of the wing to the pressure side and connected with two cables. The electrical connection is pressed in another groove milled in the suction side. Molten silicone insulates the cables from the water. On the suction side, a layer of electrically conductive carbon-based paint is sprayed on the foreseen groove. The entire wing is sprayed with several coats of white paint until no defects are visible. Finally, TSP is sprayed on the suction side and the surface is polished. The properties of the luminescent paint are described in detail by Ondrus et al. 2015. The surface roughness is measured with a Perthometer S2 at R_a=0.042 µm. The TSP film thickness is measured using a QNIX 1500. The gauge requires a metallic coated surface. Therefore, the temperature sensitive coating thickness is read from the aluminum calibration coupons. This is measured to an approximate 100µm. The electrical resistance of the heating layer at a temperature of 20°C is 28.57Ω.

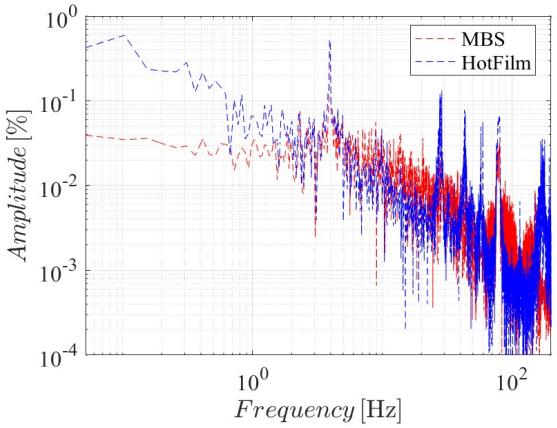

Fig. 2. Velocity tow oscillations spectrum acquired using hot-film anemometry and a magnet band sensor (MBS).

The foil is installed vertically in the towing tank. The height is adjusted to minimize the distance between the bottom surface and tank bottom. Additionally, a brush is fixed to the lower surface of the wing to reduce momentum exchange between the suction and pressure sides. The upper surface is connected to a 400 mm wide and 60 mm high glass disk to reduce the effects of water waves on the flow.

3. The illumination system and the camera

Six UV-LEDs with a peak wavelength of 405 nm are used to excite the TSP. The radiant flux is 12.1 W at a 20 ms pulse and 9 A current. The LEDs are operated in pulsed mode by one driver each. Three of the drivers are DK-136M-1 models, which are no longer in production, and the other three are DK-236, both types from Luminus Devices, Inc.. Each light source is equipped with a reflector to increase the light intensity.

A high-speed camera operated in double-frame mode is required for the measurements (Miozzi et al. 2018). The lens is equipped with a red 570 nm long-pass interference filter from Laser Components GmbH, type 570ALP 116410.

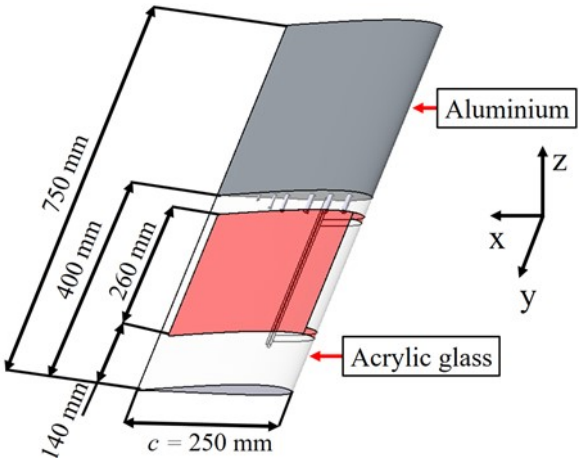

Fig. 3. CAD model of the foil with the heating element (red regions). The foil is mounted vertically in the tank.

A Programmable Timing Unit is controlled using Davis 10.2 from LaVision. The UV light pulse from the LEDs is synchronized so that it is fully contained in the first acquired image (see figure 4). The second image is timed in such a way that it includes only the light emitted from the phosphorescence.

GALA e.V., Karlsruhe, Germany, ISBN 978-3-9816764-9-5

Matlab is used to time filter the acquired data, align the images to the reference images during the towing process, and process them. The image coordinates of the centers of the eight markers inscribed on the suction side are determined with subpixel accuracy (Bitter and Kähler 2011). Thus, the model displacement and model deformation are taken into account. Furthermore, the markers are used for coordinate transformation, from an image-based to an object-based system.
As it can be seen from figure 1, the suction side is illuminated from the side. As a result, the signal is interrupted because the view of the camera and light sources is blocked by the supporting structure of the tank.

4. Data recording procedure

A total of 40 double frame images are acquired with the light sources off (dark) and on (ref) of the static wing without the heat flux. The averaged dark images are subtracted from the averaged ref images and from the images taken during the tow (run).
The ratio of ref to the run images is the so-called ratio of ratios (Liu et al. 2021). With it and the help of a calibration function, the surface temperature is finally determined. The signal is temporally filtered pixelwise by using a Savitzky-Golay smoothing filter. The cutoff frequency of the filter is at least twice as high as the highest expected vortex shedding frequency. For this, the order of the polynomial N, with which the time entries are smoothed at one location, must be specified. The Schaefer length M determines the interval width, which is necessary for the smoothing of a time entry (therefore $2M+1$). A SUSAN spatial filter is used to reduce the influence of the nonidentical camera pixels (Smith and Brady 1997).The temporal dimension is normalized by the chord length of the wing and by the tow speed ($t_{\mathrm{norm}}=(t\cdot U_\infty)/c$).
To determine the calibration function, aluminum coupons coated with TSP are placed on a Peltier element in a chamber connected to a vacuum pump. The temperature is controlled in increments of 1°C from 10°C to 40°C. After waiting one minute, 40 dark and reference double images are acquired. The resulting intensity ratios are used to define the function from which the surface temperature is obtained. The paint has shown no dependence on the static pressure. The procedure is repeated for each camera used, since different models have different interframe times.

5. Laminar separation bubble analysis using artificial heat fluxes

The project focuses on the investigation of the footprint of vortical structures shed in the shear layer of a laminar separation bubble. Their time-averaged topology has already been the focus of several studies, such as by Wynnychuk and Yarusevych 2020, Guerra et al. 2022, or Hoesslin et al. 2017. The different heat transfer rates of laminar, transitioning, and turbulent flows were used to determine the separation (x_S), transition (x_T), and reattachment (x_S) locations directly. Comparisons with other established methods such as particle image velocimetry (PIV) and thermal declining thermography have confirmed the approach with very good agreement (Wynnychuk and Yarusevych 2020). The separation and transition locations have been determined at the location of the local maximum and minimum, respectively, of the thermal gradient. The reattachment position is at the location of the local minimum of the surface temperature, downstream of the separation point. Miozzi et al. 2018 was additionally able to determine the transition point at the location of a local maximum of the standard deviation of the thermal signal. However, this could be achieved in a flow with water as the working medium, since air has a too low Prandl number.
The intensity of the heat flux must be carefully chosen. On the one hand, the amplitude of the thermal fluctuations must be amplified so that measuring instruments can detect them. On

GALA e.V., Karlsruhe, Germany, ISBN 978-3-9816764-9-5

the other hand, the flow must not be systematically influenced by the natural convection effects. The Richardson number (Ri) calculates the ratio between natural and forced convection. The number should be lower than 0.1 so that heat-induced buoyancy effects are considered negligible (Ghiaasiaan 2011). It is computed as $Ri=g\beta(T_{surface}-T_{\infty})/U^2_{\infty}$, with the gravitational acceleration g and the volumetric expansion coefficient β. In the present study, a Ri value of 0.097 can be achieved at a surface temperature that is approximately 8°C hotter than the incoming flow temperature. It is recommended to choose the sampling frequency as high as possible in order to compensate for the temporal noise of the cameras, even if the condition of the Nyquist theorem (Tropea et al. 2007) is met. The experimental parameters can be obtained from table 1.

Table 1. Experimental parameters

Parameters	Configuration 1	Configuration 2	Unit
Frame rate	300	640	Hz
Lens focal length	50	100	mm
Aperture number	2	2.8	
Sensor resolution	1342 × 1430	2048 × 1952	px
Imaging magnification	0.2142	0.1413	mm/px
Camera exposure time	700	778	µs
TSP illumination time	500	500	µs
Angle of attack (α)	2, 4, 6, 8	2, 4, 6, 8	°
Time filter Schaefer length	4	13	
Time filter order	6	3	
Time filter cut-off frequency	40.3	34.59	Hz
Heating voltage at α=2°	40,50	30	V
Heating voltage at α=4°	40,50	30	V
Heating voltage at α=6°	40,50	50	V
Heating voltage at α=8°	40,50	50	V

The experimental procedure is displayed in figure 4.

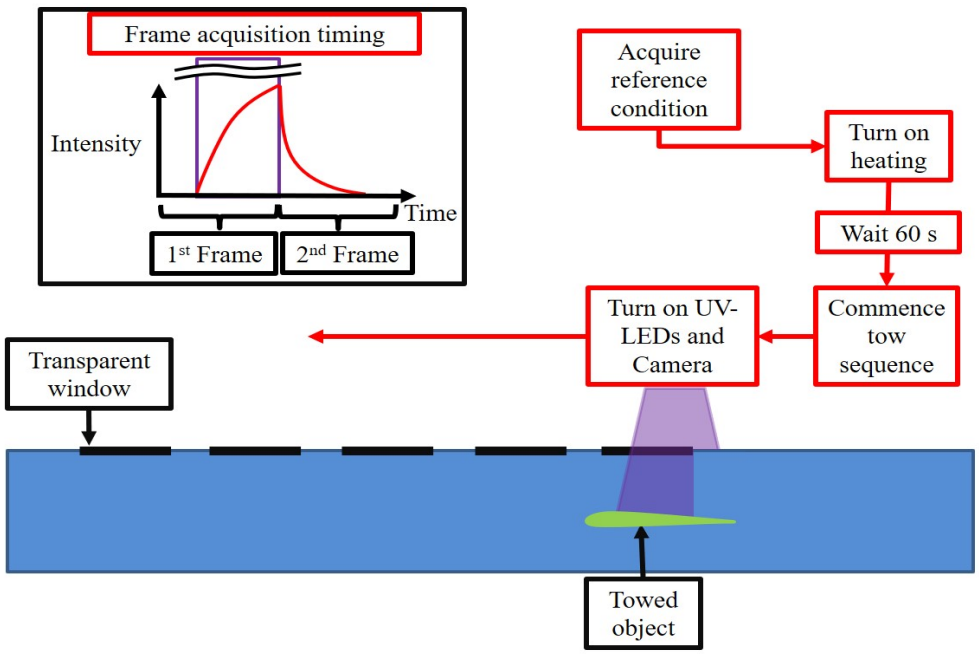

Fig. 4. Schematic of the data acquisition sequence. The towing tank is depicted from above.

GALA e.V., Karlsruhe, Germany, ISBN 978-3-9816764-9-5

With a relatively short tow duration of less than 28 convective time units, the stabilization of the thermal field must be investigated. It must therefore be recorded over the entire towing length that has optical access. The sensor resolution of the pco.Dimax S4 camera must thus be reduced. This camera model was later swapped with the Phantom V2640 to improve the detection of spontaneous events. To avoid unnecessary photodegradation, only the relevant experiments were performed at the higher sampling frequency.
The reference condition is recorded at one of the windows before the wing is moved to the end of the tank where there is no optical access. The heating is switched on and after waiting for one minute the tow sequence is initialized. Recording is started as soon as the first window is reached by the wing. The heat flux at U_{heat}=30V, 40V and 50V is $P_{heat}/A \approx 635$ W/m^2, 1129 W/m^2, and 1764 W/m^2, respectively.
Figure 5 displays the temperature distribution over time, averaged over $10 \leq x/c \leq 90$ and $-35 \leq y/c \leq 40$. At t_{norm}=0, the first window of the tank is reached. At this time, however, the airfoil has been towed at constant speed for at least 10 convective time units. At the higher angles of attack, the flow reaches a quasi-steady state more efficiently. This topic is discussed in more detail in an upcoming section.

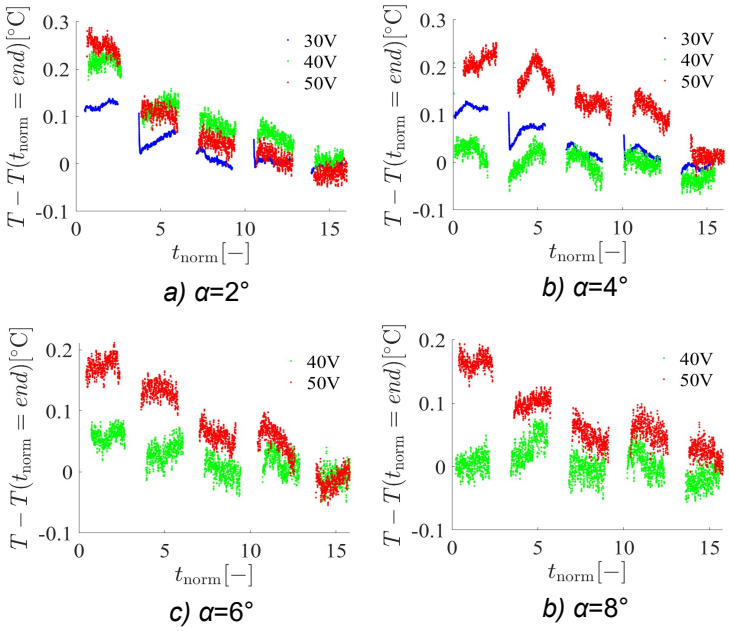

Fig. 5. Spanwise and streamwise averaged temperature distribution over time. The data at U_{heat}=40V (green dots) and U_{heat}=50V (red dots) is acquired using configuration 1 and U_{heat}=30V (blue dots) is acquired with configuration 2. The final value of every distribution is subtracted from every data set.

6. Results

A) The time-averaged thermal field

An example of the time-averaged temperature distribution is shown in figure 6 for α=6° and the highest heating voltage. The surface temperature reaches the highest values in the region between x/c=20% and x/c=40% and along the span of the heating layer. The reason for this is the relatively low wall shear stress beneath the recirculation region (Spalart and Strelets (2000)). The flow transition and the formation of the Kelvin-Helmholtz vortices force a reattachment of the flow. Thus, the surface temperature in the aft portion of the bubble decreases. A region with a higher temperature can be observed at the $x/c \approx 25\%$ and $y/c \approx -43\%$. It is outside the heating layer and occurs due to natural convection, which has a stronger

GALA e.V., Karlsruhe, Germany, ISBN 978-3-9816764-9-5

effect under the shear layer. The spraying of the carbon layer has led to a variation of the electrical resistance. This leads to heat flux inhomogeneities. These are particularly visible along the top edge of the heating layer. This does not prevent the reattachment of the flow. This can be observed due the rapidly decreasing surface temperature at $x/c \approx 40\%$.

B) The stabilization of the thermal field

The thermal field is assumed to be stable when the only surface temperature variations are caused by the fluid dynamic structures, rather than by heat conduction in or out of the wing material. Figure 7 shows the evolution of the temperature, over time. The thermal signal is averaged over $-35\% \leq y/c \leq 40\%$.

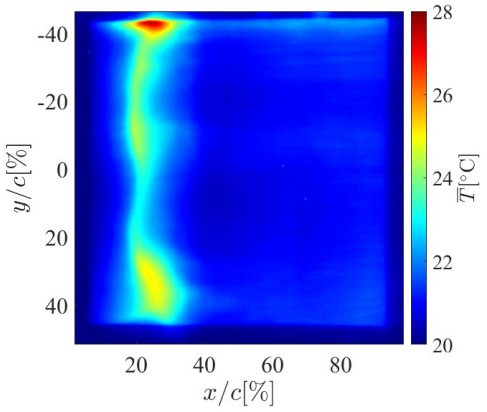

Fig. 6. Time averaged thermal field at α=6° with U_{heat}=50V

Near the leading edge, the surface temperature is low, due to the thermal boundary layer not having formed yet. At higher angles of attack and the same heating voltage, the surface temperature reaches lower values. The reason for this is the flow, which transitions further upstream. At α=8°, the separation location is so close to the leading edge of the wing that the surface temperature increases rapidly over a relatively short length. It is therefore not possible to extract the separation location from the temperature distribution. At the two higher angles of attack, the thermal field is shown at the highest heating voltage while at the lower two the lowest heating power. Nevertheless, the thermal evolution at α=6° and α=8° is less

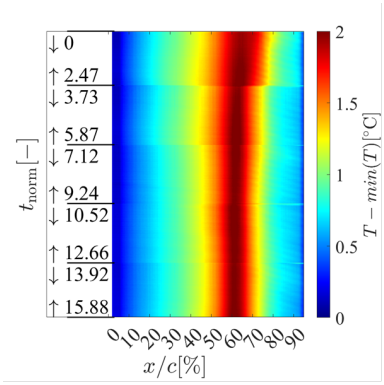

a) α=2°|U_{heat}=30V

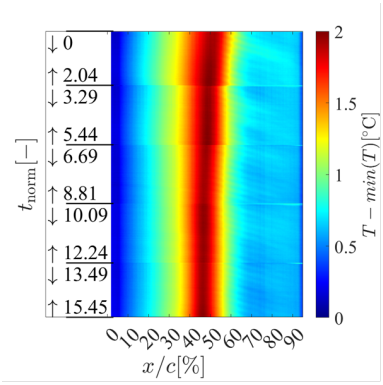

b) α=4°|U_{heat}=30V

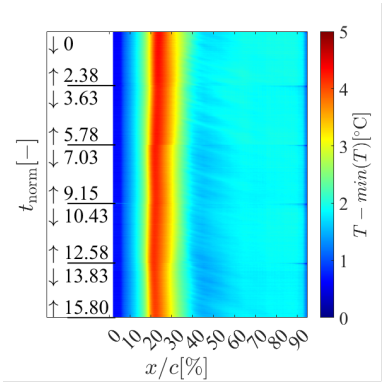

c) α=6°|U_{heat}=50V

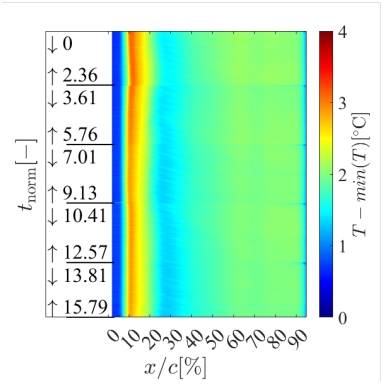

d) α=8°|U_{heat}=50V

Fig. 7. Spanwise averaged thermal signal over time at each studied angle of attack.

GALA e.V., Karlsruhe, Germany, ISBN 978-3-9816764-9-5

pronounced than at α=2° and α=4°. Due to the waiting time of one minute, the wing material absorbs thermal energy. The fluid should extract this over the tow length until a quasi-steady state is reached. To eliminate this effect, an angle-of-attack specific waiting time must be determined.

In figure 8, the same signal is reprocessed using a high-pass filter with a cutoff frequency of 1 Hz to improve the clearness of the fluctuating component of the signal. The footprints of the spanwise coherent vortices can be visualized with the approach, although the signal is averaged over $\Delta y/c$=75% of the span of the wing. This vortical structure behavior is expected since the turbulence level of the towing tank is almost zero (Istvan et al. 2018).

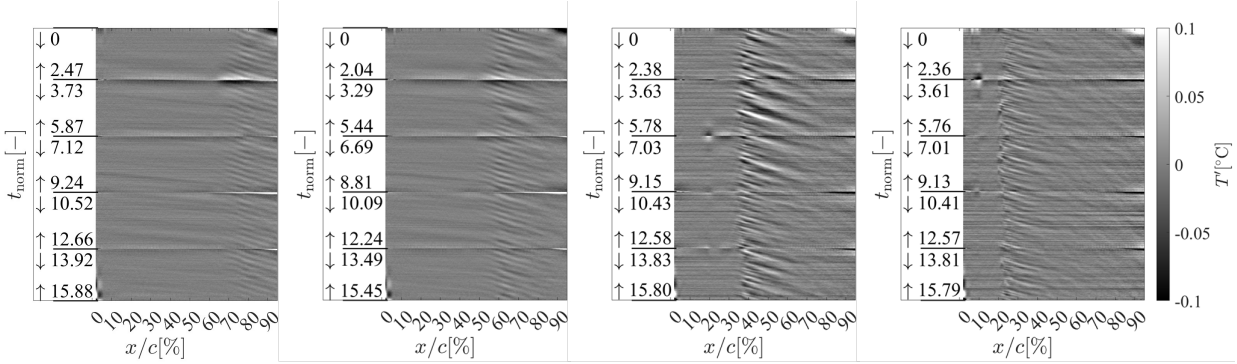

a) α=2°|U_{heat}=30V *b)* α=4°|U_{heat}=30V *c)* α=6°|U_{heat}=50V *a)* α=8°|U_{heat}=50V

Fig. 8. Spanwise averaged and high pass filtered thermal signal at each studied angle of attack. The colormap scale applies to all subfigures.

C) The time-averaged topology of the laminar separation bubble

In this section, the time-averaged topology of the bubble is compared to literature. The signal is averaged over the span as in the previous subsection and over the time entries at which the thermal field exhibits stabilization, although a perfectly stable thermal field could not be achieved. The results are shown in figure 9. At α=2° and α=8° the topology is incomplete. At the lowest angle of attack, a clear minimum in the temperature distribution could not be detected, and at the highest, the separation is too close to the leading edge of the wing.

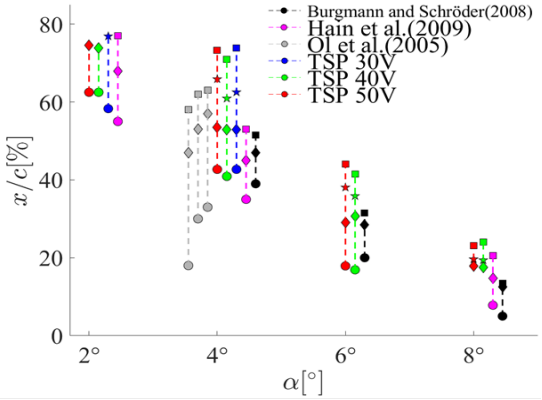

Fig. 9. Time averaged topology of the LSB at different heating powers and from literature at similar foil geometries and Re_c. Bullet, diamond, star and square represent separation, transition from literature or using the gradient method, transition computed using the standard deviation method, and reattachment locations, respectively.

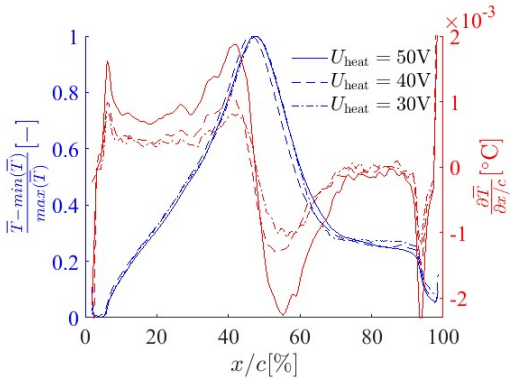

Fig. 10. Time and spanwise average surface temperature distribution and its gradient at α=4°. The line style at every heating voltage applies to the gradient lines as well.

At α=4°, the separation location is detected further downstream at all heating powers compared to data from the literature. The temperature distribution and gradient at this specific angle of attack is displayed in figure 10. The

GALA e.V., Karlsruhe, Germany, ISBN 978-3-9816764-9-5

transition location is determined by the gradient method to be closer to the separation location than to the reattachment. The literature and the result of the transition location determination method based on the standard deviation suggest the transition location closer to the reattachment point. The quality of the read is based on the assumption of a stable thermal field. This is difficult to achieve in the relatively short towing duration. Interestingly, the topologies in the present are similar to one another, although the heating power is up to 200% higher. This suggests that the heat flux itself does not affect the bubble. The lengths of the bubbles in the current experiments are comparable to those outlined in Ol et al. 2005. These were observed in experimental facilities that also have low free-stream turbulence levels.

D) The spectral content

A main criterion for the successful application of the whole experimental procedure is the resolution of the instantaneous footprints of the Kelvin-Helmholtz vortices. Based on the spectral content, the limitations of the measurement method can be analyzed. The same luminescent molecule was already able to resolve thermal fluctuations with a frequency of aproximatively 27 Hz (Capone et al. 2015) and its lifetime decay period is between 250 and 300 µs at temperatures similar to those in the present study, which is low enough to resolve the relatively low frequencies expected in the present experiments (Ondrus et al. 2015). In the current study, the capability of the single-shot lifetime method to resolve the flow features is analyzed.

The signal is extracted in the region where spanwise coherent footprints can be observed. The power spectral density spectrum is calculated using the method of Welch (Welch 1967). Here, the signal recorded at the higher sampling frequency is used. The signal is divided along the time axis into windows of 2^{11} time entries with 50% overlap. It can be processed in two ways. First, the spectral content can be calculated pixelwise and then the spectrograms are averaged over the span. Second, the thermal field can be averaged over the span of the heating layer and then the FFT is performed at an *x*-coordinate along the time axis. The results are shown in figure 11.

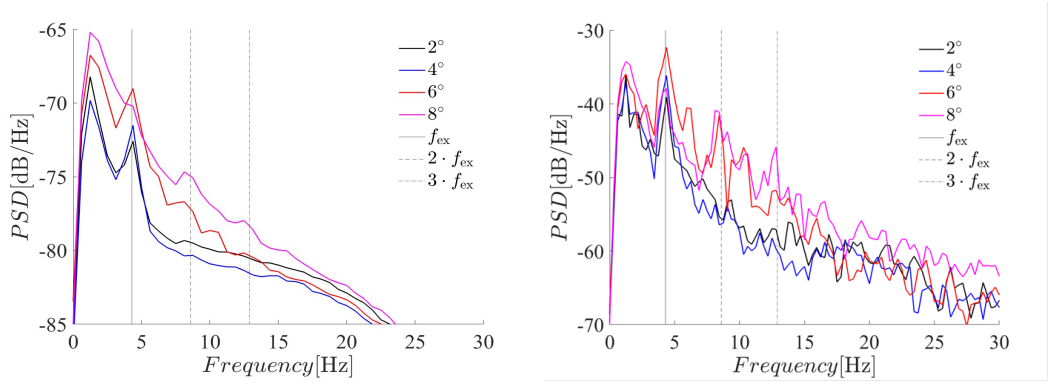

Fig. 11. Configuration 2 (see table 1): Spectral content computed pixel-wise and averaged over the span of the heating element (left) and computed after spanwise averaging the thermal signal over the span of the heating element (right) in the vicinity of the time-averaged reattachment location.

As expected, the spectrograms show similar characteristics. However, the signal averaged over the span has increased the readability of the spectral content. This is only possible in the case where spanwise coherent footprints are present. At 4.3 Hz, a high amplitude thermal fluctuation is measured at each angle of attack. This coincides with the highest amplitude velocity fluctuation shown in figure 2. At α=2° and α=4° it is the only detected fluctuation, indicating that the vortex shedding frequency is locked. At α=6°, the first harmonic and

GALA e.V., Karlsruhe, Germany, ISBN 978-3-9816764-9-5

another oscillation are also observed at approximately 6 Hz, and at α=8°, the first two harmonics are measured in addition to the excitation frequency.

7. Conclusions

The suitability of the single-shot lifetime method for resolving the footprints induced by laminar separation bubbles at low turbulence levels was analyzed. The reason for using the lifetime method instead of intensity is the unstable illumination condition in an open surface towing tank. The artificial heat flux generated by a sprayed electrically conductive heating layer increased the amplitude of the thermal fluctuations enough that the propagation of Kelvin-Helmholtz vortices could be observed. This could be achieved even when the thermal signal is averaged over $\Delta y/c$=75% of the span of the heater. This is only possible if the vortices themselves have a high level of spanwise coherence. Thus, averaging allows the spectral content to be analyzed in more detail.
Different heating powers are used and their influence on the bubble topology and on the thermal evolution over time are analyzed. At higher angles of attack, the thermal field stabilizes earlier and the averaged topologies are similar except for α=2°.
Harmonic excitation of the tow system with a frequency of 4.3 Hz and an amplitude of 0.52% of the average tow velocity locks the vortex shedding frequency at α=2° and α=4°. At α=6° the first harmonic is additionally detected and at α=8° the second one is detected as well.

Acknowledgements

This work has been supported by the Deutsche Forschungsgemeinschaft (DFG, German Research Foundation), grant number KA1808/25-1. The authors would like to thank Carsten Fuchs (DLR) for the surface preparation and Dr. Marco Costantini, Dr. Massimo Miozzi, Dipl. -Ing. Wolfgang Dierl and Prof. Serhiy Yarusevych for the insightful conversations and constructive criticism.

References

Bitter M., Kähler C.J., 2011: Optische bestimmung von Oberflächendruck- & Temperatureverteilung am NACA Profil im Unter- und Transschal. GALA - Lasermethoden in der Strömungsmesstechnik 19. Ilmenau, Deutschland.
Burgmann S., Schröder W., 2008: Investigation of the vortex induced unsteadiness of a separation bubble via time-resolved and scanning piv measurements. Experiments in Fluids 45:675–691. https://doi.org/10.1007/s00348-008-0548-7
Capone A., Klein C., Di Felice F., Beifuss U., Miozzi M., 2015: Fast-response underwater tsp investigation of subcritical instabilities of a cylinder in crossflow. Experiments in Fluids 56:196
Ghiaasiaan S. (ed) (2011) Convective heat and mass transfer. Cambridge University Press, Cambridge, Massachusetts, U.S.A.
Guerra A., Hosseinverdi S., Fasel H., 2022: Unsteady behavior of a laminar separation bubble subjected to wing structural motion. AIAA SCITECH 2022 Forum https://doi.org/10.2514/6.2022-2331
behavior of a laminar separation bubble subjected to wing structural motion. AIAA SCITECH 2022 Forum https://doi.org/ 10.2514/6.2022-2331
Hain R., Kähler C.J., Radespiel R., 2009: Dynamics of laminar separation bubbles at low-reynolds-number aerofoils. Journal of Fluid Mechanics 630:129–153. https://doi.org/10.1017/S0022112009006661
von Hoesslin S., Stadlbauer M., Gruendmayer J., Kähler C.J., 2017: Temperature decline thermography for laminar–turbulent transition detection in aerodynamics. Experiments in Fluids 58:129. https://doi.org/10.1007/s00348-017-2411-1
Lemarechal J., Klein C., Henne U., Puckert D.K., Rist U., 2018: Spatially and temporally resolved visualization of turbulent spots in Blasius boundary layer transition. 18th International Symposium on Flow Visualization.

GALA e.V., Karlsruhe, Germany, ISBN 978-3-9816764-9-5

Liu T., Sullivan J., Asai K., Klein C., Egami Y., 2021: Pressure and Temperature Sensitive Paints, 2nd Edition. Experimental Fluid Mechanics, ISBN 978-3-030-68055-8.
Miozzi M., Capone A., Constantini M., Fratto L., Klein C., Di Felice F., 2018: Skin friction and coherent structures within a laminar separation bubble. Experiments in Fluids (2019) 60:13. https://doi.org/10.1007/s00348-018-2651-8
Istvan M., Yarusevych S., 2018: Effects of free-stream turbulence intensity on transition in a laminar separation bubble formed over an airfoil. Experiments in Fluids 59. https://doi.org/10.1007/s00348-018-2511-6
Ondrus V., Meier R., Klein C., Ulrich H., Schäferling M., Beifuss U., 2015: Europium 1,3-di(thienyl)propane-1,3-diones with outstanding properties for temperature sensing. Sensors and Actuators A: Physical 233:434–441
Ol M., McAuliffe B., Hanff E., Scholz U., Kähler C.J., (2005) Comparison of Laminar Separation Bubble Measurements on a Low Reynolds Number Airfoil in Three Facilities. 35th AIAA Fluid Dynamics Conference and Exhibit., 6–9 June 2005
Savitzky-Golay Filter, 2011: What is a Savitzky- Golay filter? IEEE SIGNAL PROCESSING MAGAZINE. https://inst.eecs.berkeley.edu/~ee123/sp18/docs/SGFilter.pdf. Accessed on 25.05.2023
Spalart P, Strelets M (2000) Mechanisms of transition and heat transfer in a separation bubble. Journal of Fluid Mechanics 403:329–349
Tropea C., Yarin A., Foss J. (eds), 2007: Springer handbook of experimental fluid mechanics. Springer-Verlag, Heidelberg, Berlin, Germany
Welch P., 1967: The Use of Fast Fourier Transform for the Estimation of Power Spectra: A Method Based on Time Averaging Over Short, Modified Periodograms. IEEE Transactions on audio and electroacustics, AU-15:70–73
Wynnychuk D., Yarusevych S., 2020: Characterization of laminar separation bubbles using infrared thermography. AIAA Journal 58. https://doi.org/10.2514/1.J059160

GALA e.V., Karlsruhe, Germany, ISBN 978-3-9816764-9-5